5ICEGE
5th International Conference on Earthquake Geotechnical Engineering
January 2011, 10-13 | Santiago, Chile
Paper No. SEOTH

SPATIAL EXTENT OF LIQUEFACTION HAZARD USING DATA FROM THE 1995 HYOGO-KEN NANBU EARTHQUAKE IN KOBE, JAPAN

Thomas OOMMEN[1], Eric THOMPSON[2], Hajime TANAKA[3], Laurie G. BAISE[4], Yasuo TANAKA[5], Robert E. KAYEN[6]

ABSTRACT

Using a rich dataset associated with the 17 January 1995 Hyogo-ken Nanbu earthquake (M = 6.9), we explore the predictability of liquefaction surface effects using the liquefaction potential index (LPI) across several geologic units. The Hyogo-ken Nanbu earthquake is one of the best studied earthquakes both due to the extensive damage that resulted from the event and the subsequent data collection efforts. Extensive geotechnical and earthquake-induced-damage data were collected after the event but have remained generally unavailable to the wider research community. The data include geotechnical, geographic, geological, and earthquake damage data. The geotechnical data include the Jibankun database with over 7000 borings with stratigraphic descriptions, related in-situ and laboratory tests, and velocity profiles. We have used the dataset to investigate the relationship between strong ground motions, geology, liquefaction potential index (LPI), and the observed surficial liquefaction features. Liquefaction hazard is calculated from SPT N-value with a combination of the Simplified Procedure for liquefaction potential and the LPI. The majority of observed liquefaction features occur in the reclaimed land where sandboils cover 19.4% of the surface. In order to test the accuracy of the LPI classifications for identifying locations of observed liquefaction zones, we calculate the percent of true predictions of liquefactions (TPL) and false predictions of liquefactions (FPL) for different surficial geologic units. Given the assumptions used in this analysis, the LPI has poor predictive power of observed liquefaction features (only 18.8% TPL for the very high LPI category). The spatial distribution of TPL and FPL indicate that the poor performance of LPI is related to subtle differences in materials across geologic units. In order to investigate the relationship between LPI at a borehole location and nearby observed liquefaction features, we evaluate three different sandboil buffer distances (0 m, 100 m, 200 m) for classifying locations as liquefied or nonliquefied. As the buffer distance increases, so does the percentage of boreholes that are classified as liquefaction sites. A buffer distance of roughly 100 m leads to 83% true predictions of liquefaction (TPL) in the very high LPI category and 56% true predictions of nonliquefaction (TPN) in the nonliquefied LPI category, leading to a balance between TPLs and TPNs. When a buffer zone of 200 m is used, the TPL for the very high LPI category jumps to 92%. This increase in accuracy for identifying liquefaction locations comes at the cost of less accuracy at identifying nonliquefaction locations (41% for the nonliquefied LPI category.

Keywords: Kobe, liquefaction, database

---

[1] Assistant Professor, Department of Geological and Mining Engineering and Sciences, Michigan Technological University.
[2] Postdoctoral Researcher, Department of Civil an Environmental Engineering, Tufts University.
[3] Visiting Scholar, Department of Civil an Environmental Engineering, Tufts University.
[4] Associate Professor, Department of Civil an Environmental Engineering, Tufts University.
[5] Professor, Research Center for Urban Safety and Security, Kobe University.
[6] Research Civil Engineer, Coastal and Marine Geology, United States Geological Survey.

INTRODUCTION

The 17 January 1995 Hyogo-ken Nanbu earthquake (M = 6.9) is an extremely important event for civil engineers and seismologists concerned with earthquake hazards. The amount of damage caused by the event far exceeded what would be expected for a typical event of this magnitude. This damage can be attributed to "basin-edge" effects (Pitarka et al., 1998), widespread liquefaction (Elgamal et al., 1996), and site amplification (Iwata et al., 1996).

The basin-edge effects refer to the influence of the seismic impedance contrast at the edges of the sedimentary basin. The depth of the sedimentary basin in Kobe is on the order of 2-3 km deep. The elongated linear "disaster belt" of intense damage in Kobe is caused by the amplification of seismic waves that results from the constructive interference between the horizontally propagating basin-edge diffracted waves with the primary S wave, propagating upward from the bottom of the basin (Pitarka et al., 1998). Similarly, the local geotechnical soil conditions caused increased amplifications of seismic waves of interest to engineers. The local site conditions cause frequency-dependent amplifications at soil sites that are from 3-20 times larger than the ground motions at rock sites (Iwata et al., 1996).

The city of Kobe has built a geotechnical database system, locally known as "Kobe Jibankun", to study the earthquake damage from the 1995 earthquake. The Jibankun database consists of over 7,000 boreholes, representing a public-private partnership between the city of Kobe and local engineering companies. The information contained in each borehole is variable. Most boreholes contain Standard Penetration Tests (SPT) which measure the blow counts (N-value) with depth. Additionally, descriptions of the stratigraphy are generally available along with measurements of the depth to the water table. In many cases, grain size distributions and water content data are also available.

The Jibankun database was translated into English and imported into an online database for visualization and analysis (http://gdc.cee.tufts.edu/databases). The earthquake effects data are an extremely valuable component of the Jibankun database. In this paper we focus on the observations of liquefaction by comparing these observations to the liquefaction potential index (LPI; Iwasaki et al., 1982) computed from the SPT boreholes. We are interested in testing 1) how accurate the LPI is at predicting locations of liquefaction during an earthquake and 2) what sandboil buffer distance is appropriate for separating liquefied and nonliquefied materials.

METHODS

Data Selection Criteria

Although the Jibankun database contains 7,209 boreholes, we cannot use all of them for this analysis. We remove boreholes that are located in water because even if sandboils occurred, they would not be identified with aerial photographs. We also excluded boreholes where the water table depth is not known, where the depth of the borehole is less than 10m, where the seismic intensity is not known, and where the stratigraphy is not known. The peak horizontal accelerations (a_{max}) for the borehole locations were estimated from the approximations established by the Japan Meteorological Agency (JMA) based on JMA-seismic intensity scale (Fujimoto and Midorikawa, 1999). The JMA-seismic intensity scale is analogous to the Modified Mercalli Intensity (MMI) scale. We prefer the JMA values over an empirical ground motion prediction equation (GMPE) because a GMPE cannot account for the basin edge effects that were so prevalent in this event. We used a_{max} values of 4 m/s^2, 3.25 m/s^2, and 1.65 m/s^2 for

corresponding JMA-seismic intensities of 7, 6, and 5 respectively. After applying the various exclusion criteria, 2,684 boreholes were selected for the LPI analysis.

Computing Liquefaction Potential Index

LPI is a measure of the effects of liquefaction based on the severity of liquefaction and the depth and width of the liquefiable zones. We evaluate LPI for the top 20m of a soil profile. We compute the LPI based on the factor of safety (FS) and compute the FS with the simplified approach proposed by Seed and Idriss (1971). The cyclic stress ratio (CSR) for each borehole profile is

$$\mathrm{CSR} = 0.65\left(\frac{a_{\max}}{g}\right)\left(\frac{\sigma_{\mathrm{V0}}}{\sigma'_{\mathrm{V0}}}\right)r_d\,, \tag{1}$$

where $a_{\max}$ is the peak horizontal acceleration, g is the acceleration of gravity, σ_{V0} is the total overburden stress, σ'_{V0} is the effective overburden stress, and

$$r_d = \begin{cases} 1.0 - 0.00765z & \text{for} \quad z \le 9.15\,\mathrm{m} \\ 1.174 - 0.0267z & \text{for} \quad 9.15\,\mathrm{m} < z \le 23\,\mathrm{m} \end{cases}, \tag{2}$$

where z is the depth beneath ground surface in meters.

We compute the cyclic resistance ratio (CRR) with the clean-sand base curve for a magnitude of 7.5 and normalized blow counts as recommended by Youd et al. (2001):

$$\mathrm{CRR}_{7.5}^{SPT} = \frac{1}{34 - (N_1)_{60}} + \frac{(N_1)_{60}}{135} + \frac{50}{[10(N_1)_{60} + 45]^2} - \frac{1}{200}\,, \tag{3}$$

where $\mathrm{CRR}_{7.5}^{SPT}$ is the CRR for SPT, and $(N_1)_{60}$ is the corrected SPT blow count (<30). The corrected SPT blow count is computed by correcting for the overburden pressure using the correction factor proposed by Kayen et al. (1992). We use the Robertson and Wride (1998) correction for SPT N values and the Arion et al. (2007) correction for different countries.

We estimate the liquefaction hazard with the factor of safety against liquefaction (FS) by scaling the CRR to the appropriate magnitude:

$$\mathrm{FS} = \left(\frac{\mathrm{CRR}_{7.5}}{\mathrm{CSR}}\right)\mathrm{MSF}\,, \tag{4}$$

where CSR is computed from equation 1, CRR is computed from equation 3, the cyclic resistance ratio for a magnitude 7.5 earthquake is $\mathrm{CRR}_{7.5}$, and the MSF is the magnitude scaling factor. We use the MSF recommended by Youd et al. (2001):

$$\mathrm{MSF} = 10^{2.24} / M_W^{2.56}\,, \tag{5}$$

where the moment magnitude $M_W = 6.9$.

We then compute the LPI with the Iwasaki et al. (1982) method, which is defined as

$$\mathrm{LPI} = \int_0^{20} F_{\mathrm{L}} w(z)\,\mathrm{d}z, \tag{6}$$

where the integration is over the depth z, $w(z) = 10 - 0.5z$, and we define F_{L} following Sonmez (2003):

$$F_{\mathrm{L}} = \begin{cases} 0 & \text{for} \quad \mathrm{FS} \geq 1.2 \\ 2\times10^{6}\,\mathrm{e}^{-18.427\mathrm{FS}} & \text{for} \quad 1.2 \geq \mathrm{FS} \geq 0.95 \\ 1 - \mathrm{FS} & \text{for} \quad \mathrm{FS} \leq 0.95 \end{cases}. \tag{7}$$

The liquefaction potential index classifications are given in Table 1. The subsurface materials have all been assigned a geologic classification according to the borehole logging and are given in Table 2. The classification in Table 2 consists of two parts: (1) a capital letter that designates the age of the material, followed by (2) a lowercase letter that designates the type. We assume that only the geologic classes fill (B), fill sand (Bs), and Holocene sand (As) are liquefiable. In the integration of the LPI values, geologic classes other than these are assumed to be non-liquefiable and are assigned a FS = 1.2. The interpolation of the FS values for the integration of LPI can be completed a number of different ways. Lenz and Baise (2007) compared three different interpolation approaches and concluded that the difference in the calculated LPI values was insignificant with less than 0.5% change. Therefore in this paper, we assume that the FS values can be linearly interpolated across the borehole profile.

Table 1. LPI classification categories

LPI	Classification
0	Nonliquefiable
0 < LPI ≤ 2	Low
2 < LPI ≤ 5	Moderate
5 < LPI ≤ 15	High
15 < LPI	Very High

Table 2. Geologic classes based on the age and type of the material

	Unclassified	Gravel	Sand	Clay/Silt	Peat	Volcanic Ash	Marine Clay
Fill	B	Bg	Bs	Bc	Bp		
Holocene		Ag	As	Ac	Ap		A(Ma13)
Pleistocene		Dg	Ds	Dc	Dp	Dt	D(Ma12)
Osaka Group		Og	Os	Oc	Op	Ot	

Defining Occurrences of Liquefaction and Non-liquefaction

The empirical observations that we use to assess the accuracy of LPI are the observations of liquefaction (sandboils) that have been identified from post-earthquake areal photographs (Hamada et al, 1995). Thus, it is easy to define a true prediction of liquefaction (TPL) as a location where the LPI predicts

liquefaction (LPI classes: high and very high) when sandboils have been observed. Analogously, it is easy to define a false prediction of non-liquefaction (FPN) a location where LPI does not predict liquefaction (LPI class: low and non-liquefiable) but sandboils have been observed.

True predictions of non-liquefaction (TPN) and false predictions of liquefaction (FPL) are more difficult because these classifications require that we define an observation of nonoccurrence of liquefaction. The absence of sandboils does not guarantee that liquefaction did not occur. Thus we must devise some heuristic method of classifying locations where it is most likely that liquefaction did not occur. In this paper we propose a buffer distance method in which we assume that any borehole that is larger than an assumed distance from an observed sandboil did not liquefy. We test buffer zones of 0 m, 100 m, and 200 m. For example, using a 200 m buffer zone, a TPN is a borehole with LPI class low or non-liquefiable that is further than 200 m from an observed sandboil and a FPL is a borehole with LPI class of high or very high that is further than 200 m of an observed sandboil.

When evaluating the results, it is important to remember that TPL and TPN are directly related to FPL and FPN values (i.e. TPL%+FPL%=100% and TPN%+FPN%=100%). We only report TPL and TPN because FPL and FPN are easily computed by the reader.

RESULTS

Figure 1 is a map of the Kobe region showing the surficial geology units from the "Active Fault Map in Urban Area" published by the Geographical Survey Institute of Japan at 1:25,000 scale. This also shows the observations of liquefaction and the LPI classifications at each borehole. We see that the very high LPI category is found primarily in the reclaimed land and appears to be clustered near observed sandboils. Although qualitative visual comparisons can be informative, we also assess the accuracy of LPI using quantitative measures by comparing the locations of LPI class values with observed liquefaction features.

Of the 2,684 boreholes in our analysis, 560 are classified as non-liquefiable, 484 are classified as low LPI, 711 are classified as moderate LPI, 817 are classified as high LPI, and 112 are classified as very high LPI. The percentage of TPL for boreholes with a very high LPI classification is 18.8%, and the percentage of TPL for boreholes with a high LPI classification is 5.0%. If the 200 m buffer zone surrounding sandboils is considered liquefiable, then the percentages of TPL for the very high and high classifications are 91.9% and 74.7%, respectively. If we consider a 100 m buffer zone as liquefiable, then the percentage of TPL for the very high and high classifications are 83.0% and 57.6%, respectively.

Using the 200 m buffer zone, the percentage of TPN is 41.7% for the low LPI classification, and the percentage of TPN for boreholes with the non-liquefiable LPI classification is 40.5%. If you decrease the buffer to 100m, so that TPN are classified as locations at least 100 m from a sandboil, the percentages of TPN for low and nonliquefiable are 57.6% and 56.1%, respectively. And with no buffer, the TPN for low and nonliquefiable are 95.0% and 94.8%. These statistics for TPL and TPN indicate that there is a trade-off in accuracy depending on what buffer zone you use. In this analysis, the 100 m buffer zone tends to balance the tradeoff between TPL and TPN classification accuracy; however, another buffer zone diameter may be appropriate if the desire is to maximize either the TPL or the TPN. The TPL and TPN statistics for three possible buffer zones are summarized in Table 3.

Liquefaction potential is often predicted by surficial geology alone, so it is interesting to look at the distribution of observed liquefaction features by geologic unit. Table 4 summarizes the percent area of observed liquefaction features in each of the five surficial geologic units. As expected, the reclaimed land has the largest liquefied area and has 19.4% area covered by sandboils. The Alluvial Lowland deposit

only has 1.0% area covered by sandboils and the remaining deposits all have less than 1.0% area covered by sandboils. We also calculate the distribution of LPI categories for each surficial geologic unit as percents within each category as a comparison to the observed surface effects as shown in Table 4. For this earthquake, the category of very high gives an accurate estimate of the percent area in each geologic unit covered by a mapped sandboil.

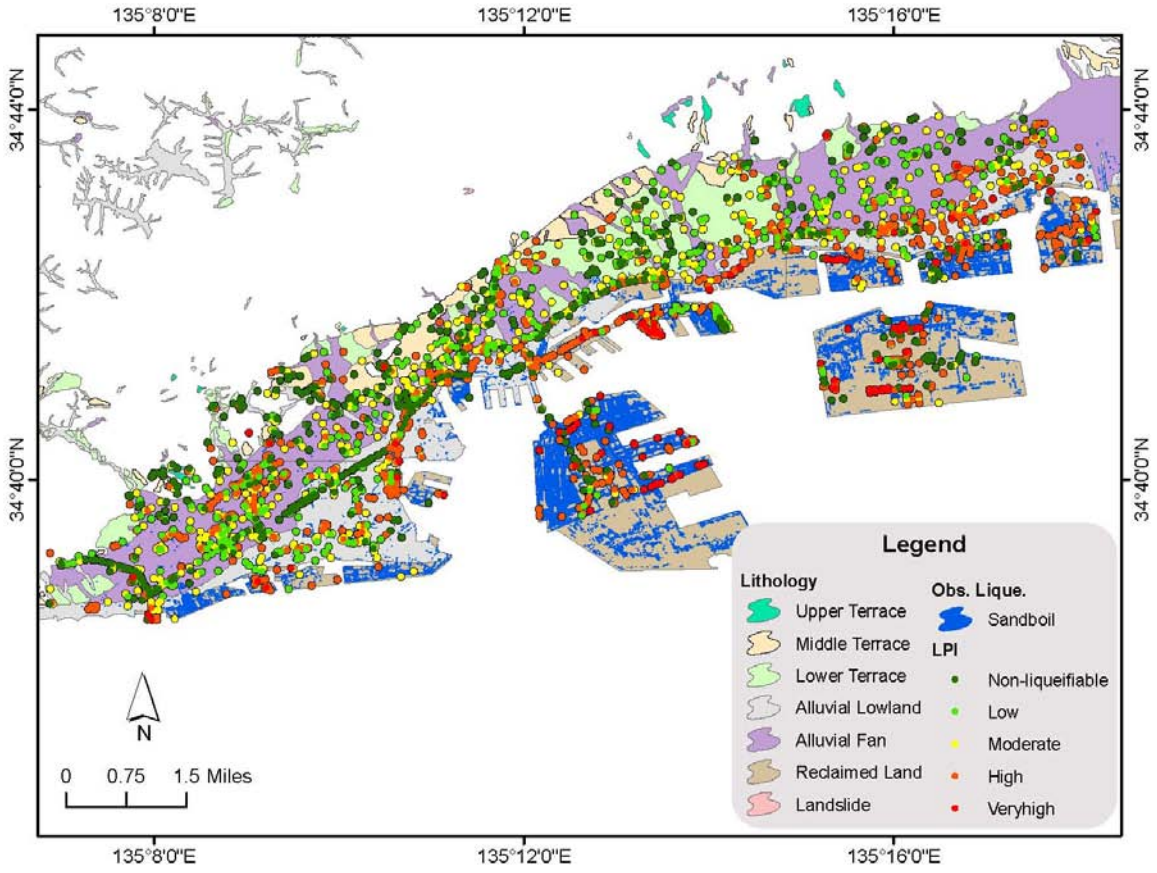

Figure 1: Map of the Kobe region showing the surficial geology units from the "Active Fault Map in Urban Area" published by the Geographical Survey Institute of Japan at 1:25,000 scale. This also shows the observations of sandboils and the LPI classifications at each borehole.

Table 3. Distribution of TPL and TPN by LPI class for different buffer assumptions

	TPL Very High LPI	TPL High LPI	TPN Low LPI	TPN NonLiq
Using no buffer zone	18.8%	5.0%	95.0%	94.8%
Using 100 m buffer zone	83.0%	57.6%	57.6%	56.1%
Using 200 m buffer zone	91.9%	74.7%	41.7%	40.5%

Table 4. Distribution of liquefaction area and LPI classes by geologic unit

Surficial Geology Unit	% area of sandboil	Very High	High	Moderate	Low	NonLiq.
Reclaimed Land	19.4%	17.5%	44.9%	7.8%	12.5%	17.3%
Alluvial Lowland	1.0%	0.7%	37.9%	27.6%	14.2%	19.5%
Alluvial Fan	0.2%	0.4%	21.4%	35.0%	24.0%	19.2%
Lower Terrace	0.1%	0.0%	25.1%	33.2%	18.9%	22.8%
Middle Terrace	0.0%	0.0%	8.2%	32.7%	23.5%	35.7%

Using a 200 m buffer zone, we evaluate the spatial distribution of the TPL, FPL, TPN, and FPN in the various LPI classes. Figure 2 is the spatial distribution of TPL and FPL for the LPI class very high. Using the 200 m buffer zone, 91.9% of the very high LPI locations are TPL. Figure 3 is the spatial distribution of TPL and FPL for the LPI class high. 74.7% of the high LPI locations are TPL; however, we also observe that the FPLs for the high LPI locations are mostly clustered in the north and north-east on the alluvial fan, lower terrace, and middle terrace. An interesting observation is that the alluvial fan towards the south has clustered TPLs whereas the same lithologic unit towards the north has mostly FPLs. This observation leads us to believe that there may be a geologic explanation for the difference in observed liquefaction in these two regions. We could investigate this through a more detailed grain-size analysis than the rough soil classification categories used to determine liquefiable and nonliquefiable materials for the LPI calculations used here.

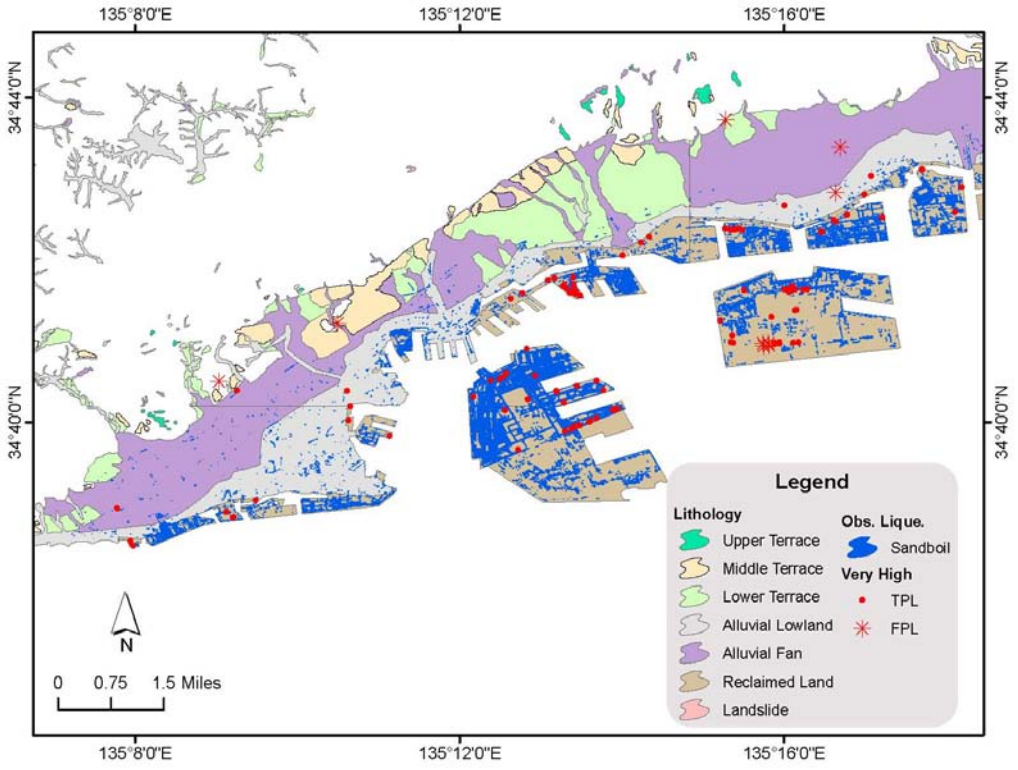

Figure 2: Spatial distribution of TPL and FPL for the LPI class very high using a 200 m buffer zone.

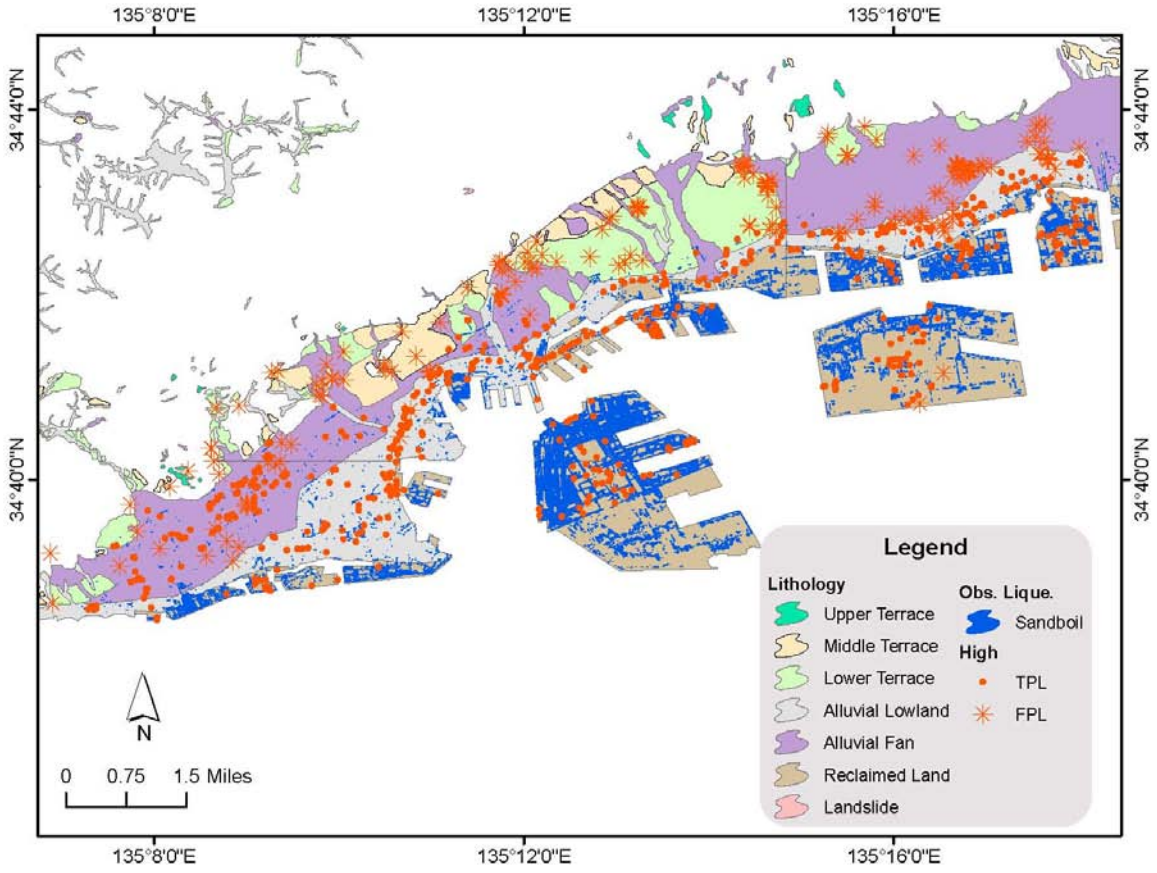

Figure 3: Spatial distribution of the TPL and FPL for the LPI class high using a 200 m buffer zone.

Figure 4 is the spatial distribution of TPN and FPN for the low LPI classification. We observe that most low LPI locations in the reclaimed land and alluvial lowland are FPN. This distribution would shift if a lower buffer zone was used. Figure 5 is the spatial distribution of TPN and FPN for the nonliquefiable LPI classification. Similar to the low LPI class, most predictions of the non-liquefiable LPI locations on reclaimed land and alluvial lowland are FPN. Figures 2-5 illustrate the trade-off that occurs between TPL and FPN for the different buffer zones. Using a larger buffer zone increases the ratio of TPL but decreases the ratio of FPN in a given geologic unit as illustrated in Table 3. From these figures, we can see that there may be geologic unit contribution to the FPL and FPN which should be investigated in future work through a more detailed soil type and grain size analysis.

CONCLUSIONS

In this paper, we analyze the liquefaction potential of the city of Kobe, Japan using the SPT data available in the Jibankun database. We then compare the predicted LPI classes to the observed liquefaction zones from the 1995 Hyogo-ken Nanbu earthquake. The majority of observed liquefaction occurs in the reclaimed land with 19.4% area covered in this geologic unit; however, liquefaction also occurs in smaller instances in the other geologic units. In this case, the ratio of very high LPI classifications in the SPT found in a surficial geologic unit mirrors the ratio of observed liquefaction to nonliquefaction by surface area. When a buffer distance is not used, the predictive ability of the LPI to identify locations of

observed liquefaction features is poor. In order to investigate whether the poor predictive power of LPI was a result of liquefiable materials near the boundaries of liquefaction features, we compare three different buffer distances (0 m, 100 m, 200 m) around the observed liquefaction zones for classifying locations as liquefied or nonliquefied. From these results, a buffer zone of roughly 100 m balances the ratio of TPL and TPN classifications; however, with the 100 m buffer zone, only 83% of the very high LPI are TPL. When a buffer zone of 200 m is used, the TPL for the very high LPI category jumps to 92%; but the percent TPN decreases.

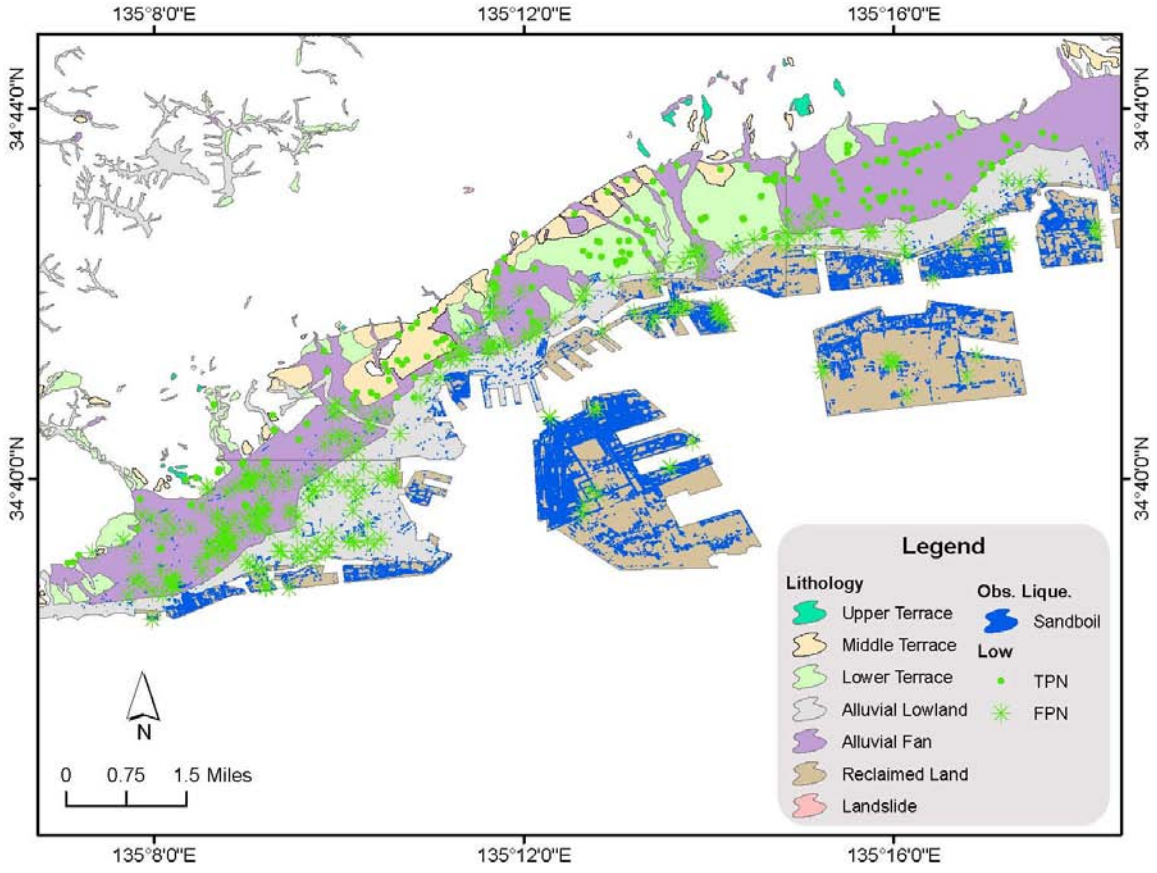

Figure 4: Spatial distribution of the TPL and FPL for the LPI class low using a 200 m buffer zone.

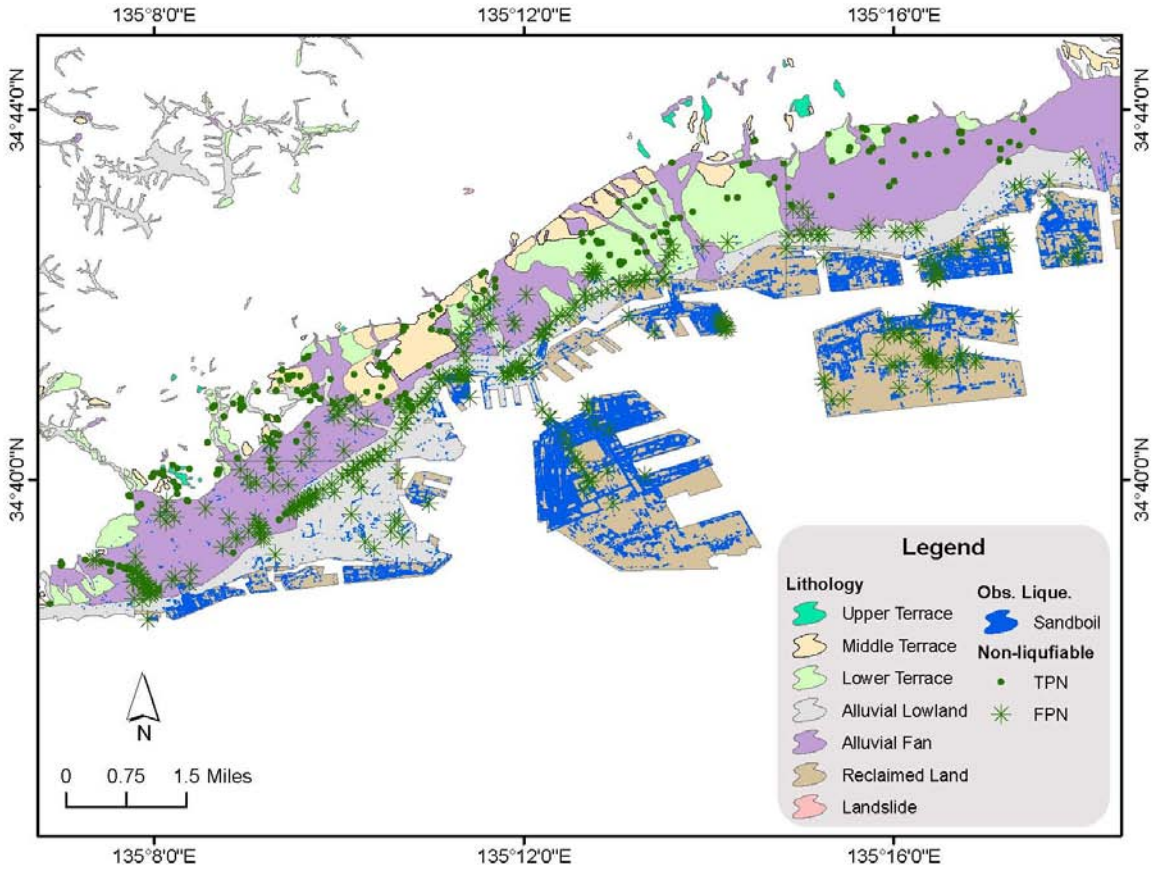

Figure 5: Spatial distribution of TPN and FPN for the LPI class non-liquefiable using a 200 m buffer zone.

ACKNOWLEDGEMENTS

We would like acknowledge the Kobe City Construction Bureau for sharing the Jibankun data with us and specifically Mr. Samata who gave permission for this research effort. Support for this research comes from the National Science Foundation CMMI Award #0547190 and the Tufts University Berger Family Technology Transfer Endowment.

REFERENCES

Arion, C., E. Calarasu, C. Neagu, and M. Tamura (2007) Geotechnical in situ investigation used for seismic design of buildings, International Symposium on Seismic Risk Reduction, paper no:2, pp. 107-120.

Elgamal, A. W., M. Zeghal, E. Parra (1996). Liquefaction of reclaimed Island in Kobe, Japan, Journal of Geotechnical Engineering, Vol. 122, pp. 39-49.

Hamada M., Isoyama, R., and Wakamatsu, K. (1995). The 1995 Hyogoken-Nambu (Kobe) Earthquake: Liquefaction, Ground Displacement and Soil Condition in the Hanshin Area. Assoc. for Development of Earthquake Prediction, Tokyo, 194 p.

Hynes L. F. and Olsen R. S (1999). Influence of confining stress on liquefaction resistance, in: Proceedings of the international workshop on Phys. and Mech. of soil liquefaction, Balkema, Rotterdam, The Netherlands, pp. 145–52.

Fujimoto, K. and Midorikawa, S. (1999). Isoseismal Map of the 1995 Hyogo-ken Nanbu earthquake estimated from Damage Distributions. J. Contrs. Struct. Eng. A1J, No. 523, 71-78.

Iwasaki, T, K. Tokida, F. Tatsuoka, S. Watanabe, S. Yasuda, H. Sato (1982). Microzonation for soil liquefaction potential using simplified methods, In: Proceedings of the third international earthquake microzonation conference, Vol. III. Seattle, WA. p. 1319–30.

Iwata , T., K. Hatayama, H. Kawase, and K. Irikura (1996). Site amplification of ground motions during aftershocks of the 1995 Hyogo-ken Nanbu earthquake in severely damaged zone - Array observation of ground motions in Higashinada ward, Kobe City, Japan, Journal of Physics of the Earth, Vol. 44, pp. 553-561.

Kayen, R. E., J. K. Mitchell, R. B. Seed, A. Lodge, S. Nishio, and R. Couninho. (1992) Evaluation of SPT, CPT, and shear wave-based methods for liquefaction potential assessments using Loma Prieta data. In: Proceedings of the fourth Japan-US workshop on earthquake resistant design of lifeline factors and countermeasures for soil liquefaction, vol. 1, p. 177-204.

Lenz, J. A., and Baise, L. G. (2007). Spatial variability of liquefaction potential in regional mapping using CPT and SPT data. Soil Dynamics and Earthquake Engineering, 27(7), 690-702.

Pitarka , A., K. Irikura, T. Iwata, and H. Sekiguchi (1998). Three-dimensional simulation of the near-fault ground motion for the 1995 Hyogo-ken Nanbu (Kobe), Japan, earthquake, Bulletin of the Seismological Society of America, Vol. 88, pp. 428-440.

Robertson, P. K., and Wride, C. E. (1998). Evaluating cyclic liquefaction potential using the cone penetration test. Canadian Geotechnical Journal, 35(3), 442-459.

Seed, H. B., I. M. Idriss (1971). Simplified procedure for evaluating soil liquefaction potential, J Soil Mech Found Div ASCE, Vol. 97, pp. 1249–73.

Sonmez, H. (2003). Modification of the liquefaction potential index and liquefaction susceptibility mapping for a liquefaction-prone area (Inegol, Turkey), Environ Geol, Vol. 44, pp. 862–71.

Youd, T. L., Idriss, I. M., Andrus, R. D., Arango, I., Castro, G., Christian, J. T., et al. (2001). Liquefaction resistance of soils: summary report from the 1996 NCEER and 1998 NCEER/NSF workshops on evaluation of liquefaction resistance of soils, J Geotech Geoenviron Eng, Vol. 127, pp. 817–33.